Received: 27 April 2023 | Revised: 14 July 2023 | Accepted: 17 July 2023

DOI: 10.1002/btpr.3382

RESEARCH ARTICLE

Cell Culture and Tissue Engineering

BIOTECHNOLOGY PROGRESS

Glass microspargers as effective frit spargers in single use bioreactors

William Tran[1] | T. Craig Seamans[1] | John S. Bowers[2]

[1]Biologics Process Research and Development, Merck & Co., Inc., Rahway, New Jersey, USA

[2]Emerging Technologies, Merck & Co., Inc., Rahway, New Jersey, USA

Correspondence
William Tran, Biologics Process Research and Development, Merck & Co., Inc., Rahway, NJ, USA.
Email: william.tran@merck.com

Funding information
Merck Sharp & Dohme LLC, a subsidiary of Merck & Co., Inc., Rahway, NJ, USA

Abstract

For multiple-use bench scale and larger bioreactors, sintered stainless steel frit spargers are commonly used as microspargers. For bench-scale single-use bioreactors (SUBs), existing microspargers are sintered plastics, such as polyethylene. However, though plastics are readily sterilized by irradiation making them convenient for single use, these designs overlook surface energy properties of the materials of construction. For these sintered plastic spargers, forces at the water-air-surface interface cause bubble coalescence, leading to lower effective mass transfer, higher gas flow rates, and differing pCO_2 profiles in cell culture. Alternative materials of construction were evaluated based on contact angle information and bubble formation observations. Sintered glass was chosen over thermoplastic polymers for higher surface wettability as described in the glass/water contact angle, its history as a commonly sintered material, and availability at costs suitable for single use applications. Glass sintered spargers and traditional stainless steel frit spargers were compared by porosity, bubble size, and k_La studies. Mass transfer (k_La) and cell culture performance equal or greater than a standard 20 µm stainless steel microsparger mass transfer efficiency was achieved by a glass frit sparger, of international porosity standard "P40" according to ISO 4793-80, which corresponds to a range of 16–40 µm.

KEYWORDS

frit, mammalian cell culture, microsparger, single use bioreactor

1 | INTRODUCTION

In mammalian cell culture, spargers are essential for sustaining cell growth by providing oxygen transfer into the liquid, as well as the removal of dissolved carbon dioxide. As cell culture processes move toward higher cell densities, demand grows for oxygen transfer. Especially for intensified perfusion culture, with target cell densities greater than 100×10^6 mL, the mass transfer efficiency of the sparger can become a limiting factor.

To reach higher mass transfer efficiencies, as measured by the mass transfer coefficient, k_La, bioreactor designs have often employed a frit sparger created from sintered beads. The beads and the void-fraction between them create a micron-sized porosity distribution that allows for smaller bubbles when gas is flowed through. Due to the smaller bubbles, a higher surface-to-volume ratio is achieved, which then correlates to higher mass transfer coefficients. Drilled hole spargers, often with sizes on the order of a millimeter in diameter, create larger bubbles and are typically used to remove carbon dioxide.

Contact angle has been shown to have a dramatic effect on the behavior of bubbles releasing from a surface.[1] Typically, contact angles are reported for a droplet of liquid on a surface in a gaseous environment. A contact angle less than 90° energetically favors the contact of liquid and solid, resulting in the droplet spreading out over the surface. A contact angle greater than 90° energetically disfavors the contact of liquid and solid, resulting in the beading up of the liquid, which creates more gas–solid contact. In contrast, when examining a

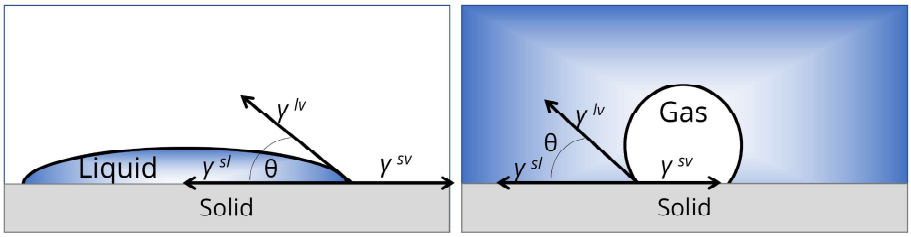

FIGURE 1 (Left) contact angle of a water droplet in air and (right) the corresponding contact angle for an air bubble in water.

gas bubble entering a liquid through a small orifice in a solid material, the observed phenomena of spreading or beading are reversed. For consistency, although this work primarily examines gas bubbles in liquid, we continue to define contact angle by the liquid–solid contact. Figure 1 shows a visual representation of contact angle for different observations of a gas–liquid–solid interface.

Wesley et al. observed that for air flowing into water through a single pore, if the liquid–solid contact is angle greater than 90°, bubbles will spread radially from the pore before releasing into the liquid. Bubbles being emitted from a surface with liquid–solid contact angle less than 90° would taper off rather than spread, thus being released from the surface faster. Consequently, bubble coalescence can also be impacted by wettability of the surface. With many pores close together, a hydrophobic surface is more likely to result in bubble coalescence.[1]

For the pharmaceutical industry, which is becoming more reliant on single use technology,[2] SUBs for mammalian cell culture from several manufacturers offer frit spargers made of sintered polymer material.[3] However, the polymer spargers do not achieve the same mass transfer efficiency comparison to stainless steel frit spargers commonly found in 3 L glass bioreactors. Despite having similar pore size distributions, the material of construction for frit spargers can have significant impacts on the size of bubbles released.[4] Consequently, variations in manufacturing variability,[5] bubble adherence, coalescence, and size distribution can adversely affect the mass transfer efficiency. This poses concerns with representative scale down models of commercial production processes.

In this work, we explore the use of glass frit spargers instead of polymer frit spargers. With a lower contact angle, and subsequently, better surface energy characteristics for bubble release, more consistent bubble size distributions are achieved. Additionally, as a material, glass is suitable for gamma irradiation and it has a manageable cost per unit for bench scale vessels.

2 | MATERIALS AND METHODS

2.1 | Glass frit sparger

Glass frit spargers were obtained from Robu, Hattert, Germany, attached to a glass tube. The frits were of borosilicate glass and manufactured to several porosity classes. Classes "P40," 16–40 µm, "Coarse," 40–60 µm, and "Extra Coarse," 170–220 µm were evaluated here. The sparger assembly was inserted into a SUB via a PG13.5 port under a laminar flow hood for this work. Further improvements included the glass frit sparger integrated in the SUB, as shown in Figure 2, so they are gamma irradiated at vessel manufacture and thus do not require utilizing a probe port. The inner diameter of the assembly was sized to allow sufficient flow and minimize dead volume in the sparger assembly. The ROBU part number selected at the end of evaluation was 18,103.

FIGURE 2 Integrated frit sparger as developed for CerCell® 3 L single-use bioreactor (CerCell A/S, Denmark).

2.2 | Characterization of sintered metal and glass frits

Scanning electron microscopy (SEM) analysis was performed by Particle Technology Laboratories. Samples were prepared by mounting to an aluminum stub using carbon tape followed by gold sputtering. SEM micrographs were taken with a JEOL NeoScope II at magnifications ranging from 30× to 4000×. A series of images were taken of the flat bottom of each diffuser, one set at increasing magnification and one set at low magnification, while scanning across the sample surface. Image analysis was performed on the latter set and the percent pore area was determined by thresholding the images to binarize the void

and solid spaces and then by quantifying the void area against the total area. This was done for each image and a mean and standard deviation were calculated for each sample.

The surface area of samples were measured via gas physisorption analysis, using the static volumetric method. The instrument used was a Micromeritics TriStar II 3020 and degassing of the sample was performed in a vacuum at room temperature for 3.5 h. The amount of Krypton that adsorbed to the surface of the samples were measured at three different pressure points, and the surface area was calculated using the Brunauer–Emmett–Teller (BET) equation.

$$\frac{1}{V_\alpha\left(\left(\frac{P}{P_0}\right)-1\right)}=\frac{C-1}{V_m C}\times\frac{P}{P_0}+\frac{1}{V_m C}, \quad (1)$$

where $\frac{P}{P_0}$ is the relative pressure, V_α is the volume of gas adsorbed, V_m is the volume of gas adsorbed to produce an apparent monolayer, and C is the BET constant.

2.3 | Visual evaluation of plastic frits, glass frits and sintered metal frits in water

In stainless steel and glass bioreactors, sintered stainless steel frits are welded to a threaded base for attaching to a dip tube. However, due to challenges machining threads on soft materials, manufacturers needed to be more creative with implementation. Various strategies were observed for implementing the microsparger, ranging from simple insertion into a silicone tube to 3D printing of a housing that would encapsulate the polymer material. Insertion into a silicone tube proved ineffective, as it easily leaked air around the sintered polymer rather than passing through it. Some of the most promising designs were a 3D printed housing that would compress a sintered polymer disk against an open orifice and a 3D printed encapsulation of a sintered polymer frit, both shown in Figure 3. For visual evaluation, the polymer disk housing was chosen, and 2 polyethylene (PE) disks with porosities of 15, 100, and 200 μm were mounted on opposite sides of the housing. Spargers were mounted in a SUB and immersed in water before sparging with gas at various flowrates. No agitation was used for visual clarity.

2.4 | Comparing bubble size distributions via focused beam reflectance measurement (FBRM)

Microspargers were attached in a vertical orientation to a polycarbonate adapter in a 3 L CerCell bioreactor operating at 200 rpm and a gassing rate of 0.01 vvm. The test liquid was 2 L of Gibco CD CHO media with 0.01% NaN_3 and measurements were conducted in an open system that was washed at the end of each experimental day. The FBRM probe was held up by a ring stand and oriented at about a 40° angle through a PG13.5 port. Measurements were taken every 10 s for about 2 h. Data was retrieved for 30 bins of chord lengths, with the width

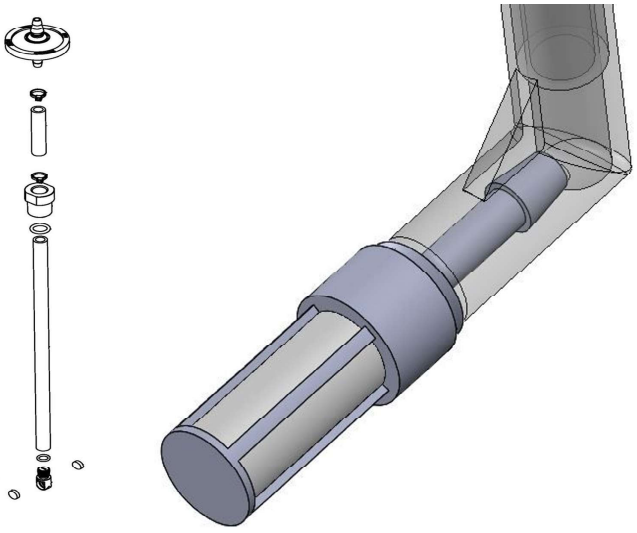

FIGURE 3 Various implementations of single use polymer microspargers. (Left) A polycarbonate tube and housing that contains openings for two disks of sintered polyethylene (right) a 3D printed casing for a sintered polymer sparger.

dependent on the total spread of values. While plotted on a logarithmic scale of bin length, histograms of chord counts were time-averaged and weighted by the square of bin length to achieve a theoretical volume-weighted distribution. Distributions were normalized such that the area under the curve is equal to 1. An average of each distribution was calculating by dividing the second moment of the unweighted distribution by the first moment of the same distribution.

2.5 | Evaluation through k_La studies

The k_La for oxygen was measured using the static gassing out method using a Sartorius bioreactor control tower (Sartorius, Goettingen, Germany) in a representative cell culture medium. Nitrogen was sparged through a 14 × 0.5 mm drilled hole sparger until %DO dropped below 10% prior to each k_La determination. Then air was sparged at fixed flowrates controlled by mass flows controllers. Agitation was set at a fixed 200 rpm, corresponding to a power per unit volume (P/V) of 40 watts per cubic meter. Oxygen fugacity was measured using a polarographic membrane oxygen probe (Mettler Toledo). The k_La was taken from slope of lines of ln(DO) versus time when the DO was between 20% and 80%. Data was fit to a power law formula that contains a term for gas flow rate in reactor volumes per minute (vvm) and a squared term to allow for curvature of the response.

$$\ln k_La = A\times\ln vvm + B\times(\ln vvm)^2 + C. \quad (2)$$

2.6 | Cell culture

Fed batch cell cultures were conducted in 3 L SUBs (CerCell A/S, Herlev, Denmark) with a 1.6 L initial working volume. The agitator was a

three-blade pitched blade operating at 200 rpm, which is approximately 40 watts per cubic meter. Dissolved oxygen was controlled by sparging with pure oxygen gas through the frit spargers being tested. Temperature was controlled by an electric heating blanket. pH was controlled within a deadband with 1 M sodium carbonate as a base, and CO_2 sparge to decrease pH. Bioreactors were controlled with MFCS software (Sartorius, Goettingen, Germany) and culture feeds were conducted by an automated sampling system (Flownamics, Madison).

3 | RESULTS AND DISCUSSION

3.1 | Polymer microspargers in bench-scale single use microspargers

Visually, the polymer spargers tested had poor control gas distribution. Gas exited from a few locations, rather than evenly dispersing across the porous surface. Most gas passed through the end of the sintered material while some was dispersed laterally. In Figure 4, larger bubbles (more than several mm in diameter) are visible flowing out the end with both a larger diameter and a greater frequency compared to the smaller bubbles (up to 2 mm diameter) escaping laterally through the side. As expected by the contact angle[1] bubbles tended to stick to the surface of the polymer frit and grow in size prior to releasing into the liquid.

Alternative porosities of sintered polyethylene (PE) were available in the form of a disk. A range of porosities were sourced to see if decreasing porosity of the sintered material could provide better dispersion of bubbles, shown in Figure 5. A 20 µm stainless steel microsparger was used as a basis of comparison while PE disks of 15, 100, and 250 µm sizes were configured for bubble testing in water.

Decreasing porosity was not sufficient to further decrease bubble sizes being emitted from the surface. The 15 µm PE disk actually produced bubbles of a similar size as the 100 µm disk, suggesting that surface energy characteristics was the dominant force in determining bubble size, rather than pore size. This was particularly clear in the figure with the 100 µm disk, where stationary bubbles on the left side do not have enough buoyant force to release from the surface at their current size. There continued to be certain pore locations that were favored, but this was particularly pronounced at the 250 µm porosity.

Initially, one can see why polymer frit spargers might be chosen for this application based on many practical characteristics. They can be low cost for single use products, are sterilizable by gamma irradiation, and they have known compatibility with mammalian cell culture for leachables and extractables. However, the gassing performance of these microspargers suggests there is much room for improvement before they are fit for use as an industry standard. At the time of writing this article, sintered polymer microspargers at the bench scale do not offer sufficient mass transfer efficiency to replace typical stainless steel sintered microspargers in intensified perfusion cell culture applications.

3.2 | Selecting a new material and an appropriate porosity

The effect of contact angle on gas bubbling through a single orifice has been well studied. Lin et al. describe the energy balance and forces associated for a bubble to release from an orifice, which includes attachment force of the bubble, forces that expand or shrink the contact base of the bubble, and the detaching force.[6] For contact angles above a 45° threshold, bubble size becomes dependent on the diameter of bubble contact base, and independent of the orifice size. Diameter of contact base increases as contact angle increases. Wesley et al. further demonstrate by using surface chemistry modifications of various silanes and thiols, that a 90° contact angle is a threshold for bubble behavior when releasing from a surface.[1] For orifices in

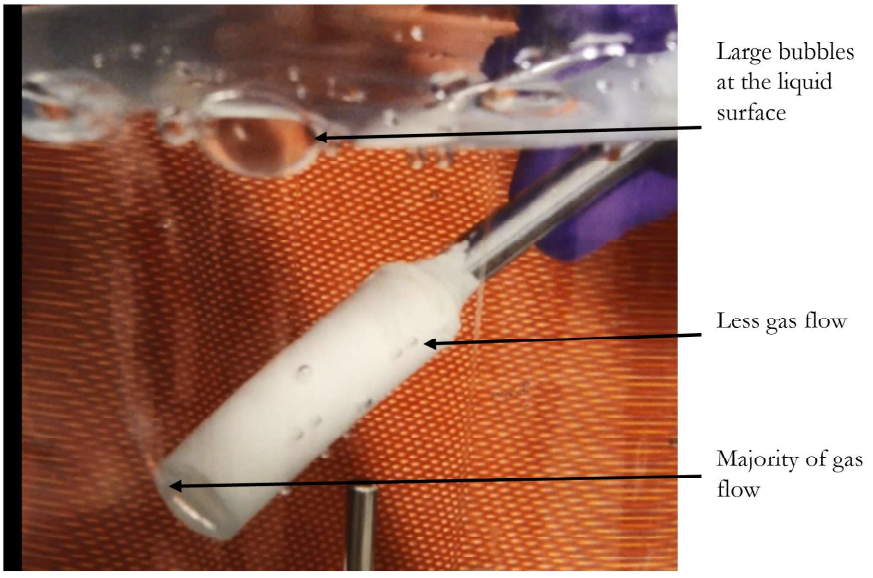

FIGURE 4 Uneven distribution of gas exiting the polymer frit. The majority of gas flowed through the end, with bubbles releasing at a higher frequency. Gas also escapes through the side surface to a lesser extent, bubbles grow in size before releasing into the liquid.

hydrophilic surfaces (contact angle <90°), smaller bubbles that taper off from the orifice were emitted. In contrast, on hydrophobic surfaces (contact angle >90°), bubbles spread out along the surface, which increases the contact base described by Lin, and ultimately emit larger bubbles.

For mammalian cell culture applications, the contact angle of cell culture medium may vary throughout a process with the addition of surfactants and with the lysis of cells. Thus, we looked for a material that has a contact angle equal to or less than that of stainless steel. Further, the material needed to be easily sourced and sintered to be effective in a single use microsparger application. It was noted that glass fits the criteria, having a contact angle less than 10°,[7] and indeed, bubbles released from the surface of a glass microsparger with smaller sizes compared to the polymer materials. Figure 6 shows a comparison of microspargers with different materials of construction, but similar porosity distributions and gas flow rates. Visible coalescence is observed on the surface of the PES sparger, with bubbles growing in size prior to releasing into the liquid. For both the stainless steel and glass spargers, bubbles release into the liquid without visibly adhering to the sparger surface first.

In order to obtain a similar bubble size distribution compared to the 20 µm stainless steel microsparger, several classes of porosity for glass microspargers were selected for study, including 16–40, 40–60, 40–100, and 170–220 µm. Despite having a similar nominal porosity, bubbles emitted from the glass 16–40 µm microsparger were smaller than bubbles emitted from the 20 µm stainless steel microsparger. The 40–60 and 40–100 µm glass microspargers were comparable to the reference. However, the 170–220 µm porosity showed significant coalescence, resulting in bubbles that were larger than those obtained from a 0.5 mm drilled hole sparger.

When comparing glass and stainless steel materials, glass has a lower contact angle, so it is not surprising that despite similar porosities, bubbles being emitted from the glass sparger could be smaller. Further, additional considerations must be taken when observing a porous material rather than a single orifice. Differences between the two sparger materials could be compounded by the effect of surface roughness on contact angle. Roughness can exaggerate the effect of surface energy on bubble formation.[8] If a contact angle is <90°, roughening will serve to reduce contact angle, whereas if a contact angle is >90°, the contact angle would be further increased. If the greater roughness of the glass material served to further decrease the contact angle relative to stainless steel, this would correspond to a smaller bubble size. Notable differences in surface roughness characteristics were shown by SEM images in Figures 7 and 8.

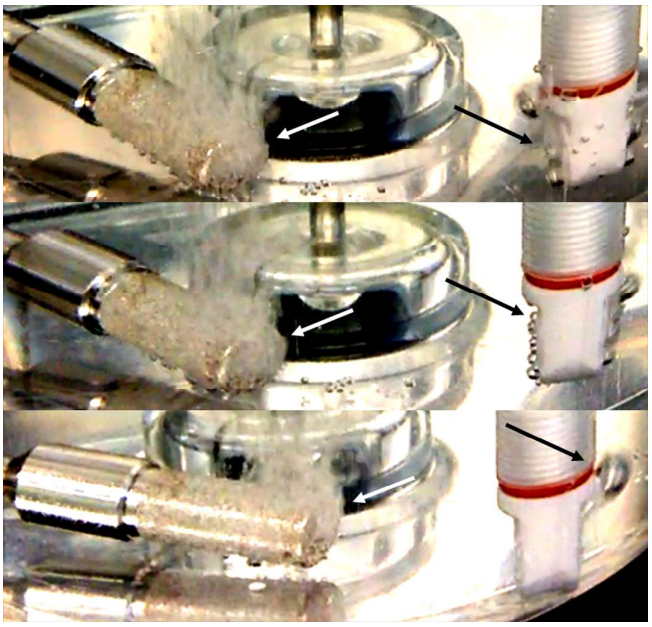

FIGURE 5 A 20 µm stainless steel microsparger in operation compared to PE disks sparging at 100 ccm flowrate. Contrast was enhanced to show bubbles. For all porosities of the PE disk spargers, the (top) 15 µm (middle) 100 µm and (bottom) 250 µm porosities produced larger bubbles. Moreover, the bubbles at the surface of the polymers tended to stick to the surface and grow in size prior to releasing into the liquid. Bubble sizes are independent of porosity of the polymer disks.

3.3 | FBRM measurements for estimating bubble size distributions

Laser backscattering techniques such as FBRM measurements have previously been used to some success for measuring the size

FIGURE 6 Bubble emission from a (left) 15 µm sintered PE disk sparger, (center) 20 µm sintered stainless steel microsparger, and (right) 16–40 µm sintered glass microsparger flowing air at 100 mL/min.

distributions of liquid–liquid emulsion droplets.[9] While concerns have been raised that the smooth surfaces of droplets lead to errors in size measurements,[10] we nevertheless wanted a screening tool to make decisions on porosity. Ultimately, the use case in cell culture systems would have many other confounding factors due to the composition of culture medium and the presence of surfactants. Observable mass transfer efficiency in a representative medium was for our final selection criterion. In future follow up studies, an investment in better techniques to measure bubble size such laser particle image velocimetry (PIV) would be of interest.

Several authors have reported methods for inverting a chord length distribution (CLD) into a particle size distribution (PSD).[11,12] In this work, the true value of the particle size is not sought after since the apparent mass transfer coefficient is a relevant proxy for cell culture applications. However, it is informative to compare the distributions of particle sizes, and to that extent, we took the average of the CLD to be weighted by particle size in our interpretation of the PSD. That is, the [1,0] average of the CLD, is proportional to the[1,2] average of the PSD.[13] Following the proportionality between the two distributions as outlined by Wynn et al., the Sauter mean diameter can be calculated from the CLD.

Sauter mean diameter is a representation of typical bubble size, typically calculated by

$$d_{3,2} = \frac{\sum_{i=1}^{\infty} d_i^3}{\sum_{i=1}^{\infty} d_i^2}, \tag{3}$$

where d_i is the diameter of the bubbles, in this case, estimated from FBRM measurements. When using the chord lengths instead of diameter, we estimate that the third moment of diameter would be proportional to the second moment of chord length, and the second moment of diameter is proportional to the first moment of chord lengths.

$$\frac{\sum_{i=1}^{\infty} d_i^3}{\sum_{i=1}^{\infty} d_i^2} \propto \frac{\sum_{i=1}^{\infty} c_i^2}{\sum_{i=1}^{\infty} c_i^1}, \tag{4}$$

where d_i and c_i are respectively the individual diameters and chords in a distribution. Chord length distributions were measured for stainless steel microspargers at 10, 20, 40, 50, and 100 μm of nominal porosity, alongside several classes of porosity for glass, including 16–40, 40–60, 40–100, and 170–220 μm.

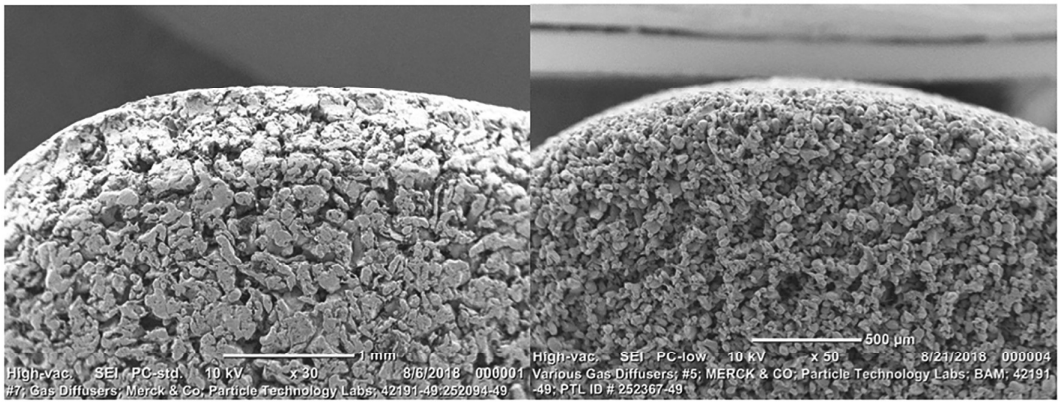

FIGURE 7 The surface of the (left) stainless steel frit also appears to have been smoothed out. Further, particles are smaller in the (right) glass, with several-fold greater specific surface area by BET isotherm (data not shown).

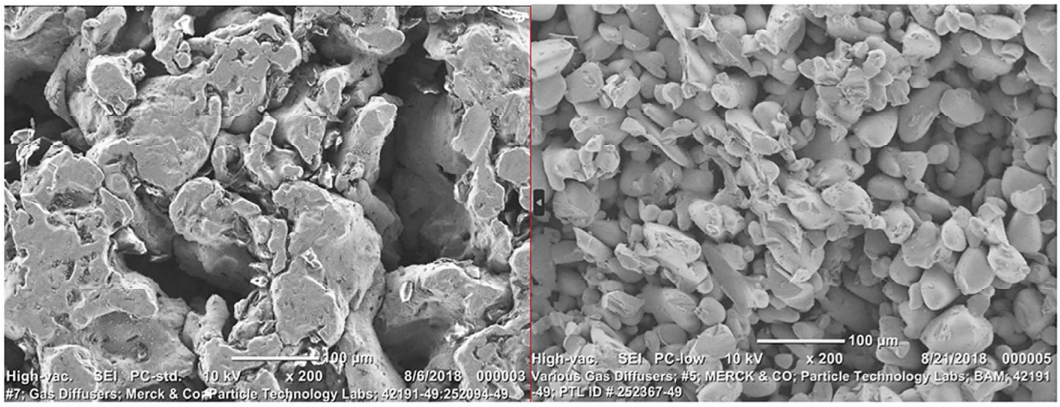

FIGURE 8 SEM image microscopy of (left) 20 μm stainless steel frit versus (Right) Porosity 16–40 μm glass frit at various magnifications.

For the stainless steel microspargers, their CLDs were not visibly different for any of the porosities tested, despite a wide range of average nominal pore sizes (Figure 9). The specific surface areas are in the range of 0.004 to 0.010 m^2/g as measured by BET isotherm (Table 1) and the Sauter mean diameter was in the range of 100–200 µm for all porosity classes.

The glass microspargers had very different CLDs with different nominal porosities. The distributions corroborate visual observations that of a greater range of bubbles sizes for different nominal porosity classes and would be expected to impact gas transfer. Further, the specific surface areas of the glass microspargers showed a wider range (0.011 to 0.060 m^2/g) compared to their stainless steel counterparts (Table 1). When plotting the Sauter mean diameter versus nominal porosity size, the glass microspargers showed a much stronger correlation compared to the stainless steel microspargers (Figure 10), where Sauter mean diameter was largely independent of the nominal porosity. Based on 95% confidence interval testing, the slope of the line of best fit between Sauter mean diameter and nominal average porosity was not substantially different from zero for stainless steel.

3.4 | k_La measurements

Gas transfer k_La measurements were taken at a fixed agitation rate with gas flow rates up to 0.1 vvm. These data correlated with FBRM measurements. The Sauter mean diameter was inversely correlated with k_La, and the stainless steel frits had similar k_La values (Figure 11).

For use in mammalian cell culture, the glass microsparger needed to provide at least the same amount of mass transfer compared to the stainless steel microsparger. Based on the measurements taken, the 40–100 µm microsparger provided comparable mass transfer compared to the 20 µm stainless steel while the 40–60 and 16–40 reach even higher mass transfer coefficients. Within the operating range tested, the k_La showed linearity with gas flow rate, which is important for consistent and predictable performance in dynamic cell culture environments.

While the glass 16–40 µm sparger can achieve high mass transfer coefficients, there are diminishing returns at high gas flow rates (Figure 12). When sparging more than 0.06 vvm, further increases in gas flow rate correspond to smaller incremental increases in mass transfer, resulting in loss of linearity in the power law fit. In contrast, linearity was maintained throughout the range tested for both the 20 µm stainless steel and 40–100 µm glass spargers. Because the dispersion of bubbles from the stainless steel microspargers is more evenly spaced across the surface, the exiting stream of bubbles could be less susceptible to coalescence behavior that has been observed at high gas flow rates.[14]

To supplement the dataset on the stainless steel microspargers, k_La data was compared to stainless steel microspargers from a 2000 L vessel. At gas flow rates less than 0.03 vvm, 50 and 100 µm stainless

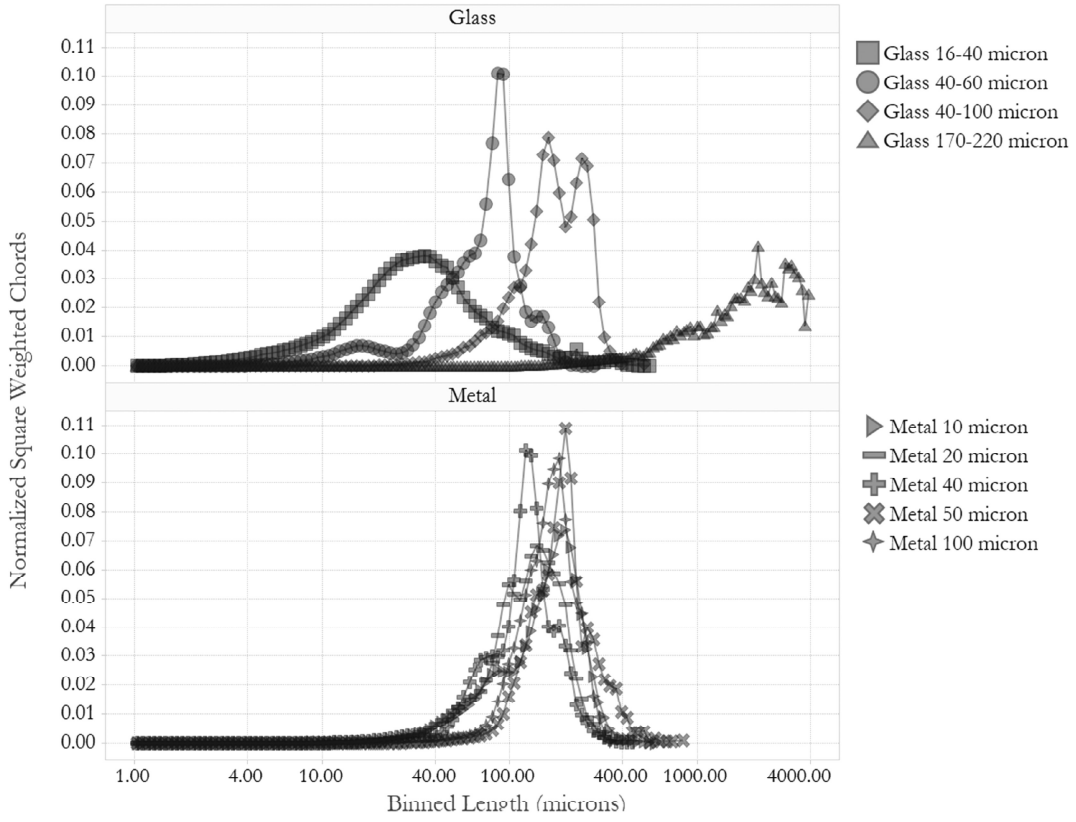

FIGURE 9 Square-weighted binned chord length distributions for various microspargers by FBRM. Glass microspargers show more differentiable distributions at different porosity classes whereas chord length distributions from the stainless steel microspargers look similar.

steel microspargers showed relatively similar mass transfer efficiencies at the 2000 scale, whereas the 20 µm microsparger provided more mass transfer.

The lack of scalability of sintered type microspargers is not unexpected, and similar issues during scale up could be expected with glass. The volumes of gas passing through limited surface areas of the spargers at the larger scales can result in the formation of a heterogeneous bubble size distribution as described by Shah et al.[15] Also, a greater tank liquid height can lead to longer residence time of bubbles. Compared to small scale, this allows more opportunity for concentration gradients within the gas bubbles to deplete. This is particularly important in mammalian cell culture, where the addition of surfactants and the pH can have implications on surface tension for the bubbles, which then impacts the size. At larger scales, SUB manufacturers could try to avoid this problem by looking for design opportunities to spread out gas entrance over a greater surface area.

TABLE 1 Specific surface areas of microspargers by BET isotherm.

Material	Nominal porosity (microns)	Specific surface area (m^2/g)
Glass	16–40	0.060
	40–60	0.029
	40–100	0.021
	170–220	0.011
Stainless steel	10	0.010
	20	0.009
	40	0.006
	50	0.006
	100	0.004

3.5 | Cell culture

It has been reported that some mammalians cells may be sensitive to high gas flow rates in the bioreactor.[16] Particularly with the small bubbles coming from a frit sparger, the cell damage is related to energy dissipation as a bubble reaches the liquid surface and bursts.[17,18] When the length scale of the energy dissipation and the length scale of the cells are of similar magnitude, rupture of the bubbles can cause damage to the cell membranes. Cell culture processes typically use pluronic in culture media to mitigate the impact, by preventing adherence of cells to bubbles, but sparger damage continues to be a recurring concern.[19]

Here, use of the glass frit sparger was evaluated in a fed-batch cell culture process to demonstrate no negative impact to cell growth from the 16–40 µm glass frit compared to the stainless steel frit (Figure 13). The 170–220 µm sparger showed significant bubble coalescence and consequently required much higher flow rates of oxygen to control at setpoint, which eventually led to excessive foaming. Total gas flow rates for the 16–40 and 20 µm stainless steel microspargers were similar, with the 40–60 µm microsparger requiring about five-fold more oxygen flow. Foaming for the 16–40 µm microsparger was less thick than foam from

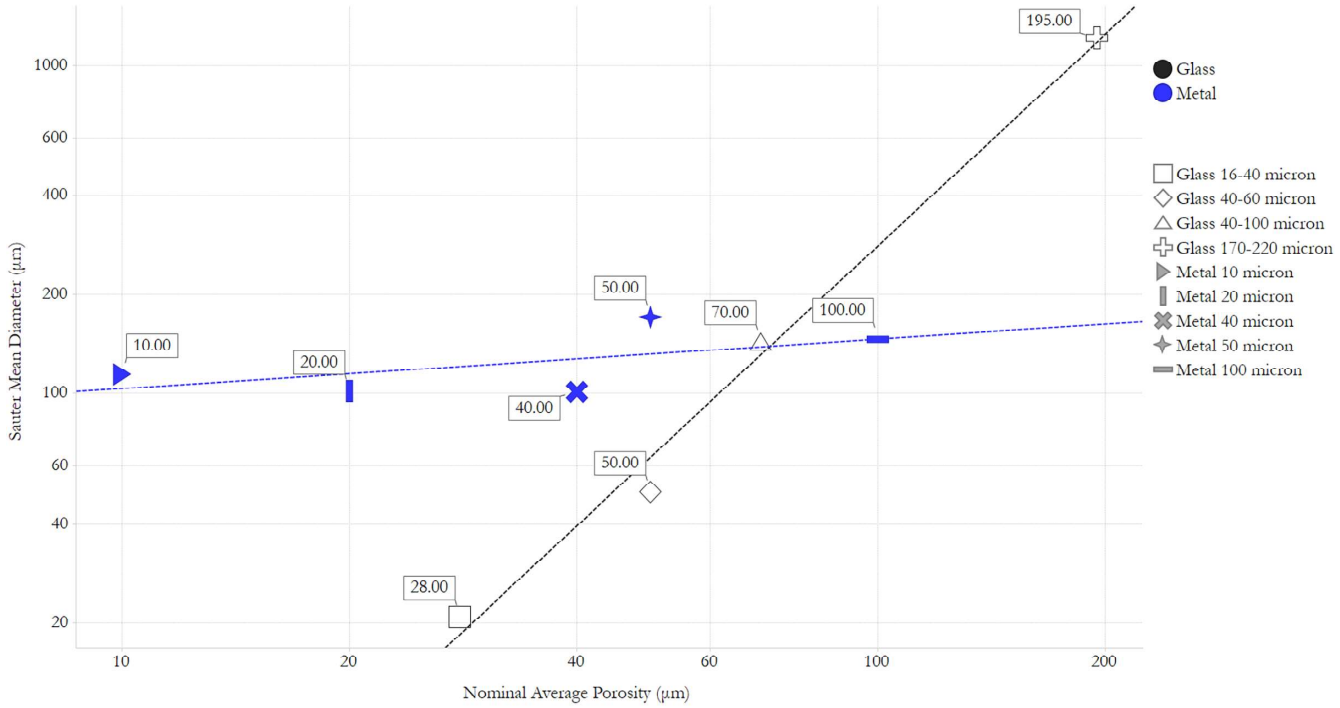

FIGURE 10 Calculated Sauter mean diameter plotted against nominal porosity. Glass microspargers showed a stronger correlation between porosity and bubble size distribution compared to the stainless steel microspargers.

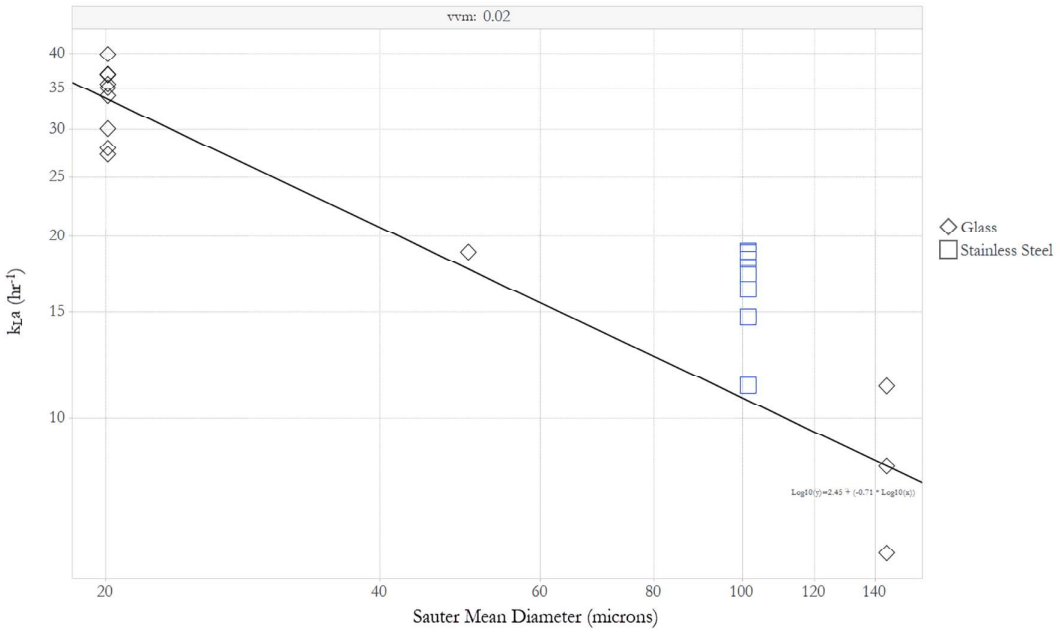

FIGURE 11 Relationship between k_La and Sauter mean diameter. k_La decreases with increasing Sauter diameter, which corresponds to lower surface-to-volume ratio for bubbles.

FIGURE 12 k_La plotted against flow rate for various porosities of microspargers. Dashed line represents glass and the solid lines represent the stainless steel microspargers. The 16–40 and 40–60 μm glass microspargers were fit using a quadratic power law. The 20 μm stainless steel and 40–100 μm glass were fit using a linear power law.

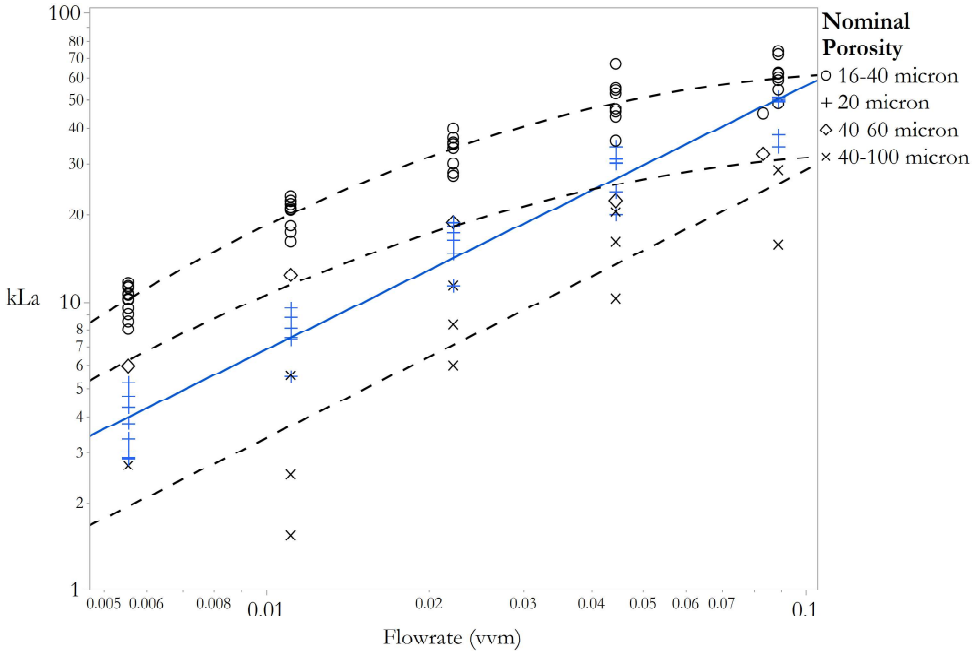

the intermediate porosities, but they were all managed successfully by the same antifoam addition strategy.

4 | CONCLUSION

In this study, the use of single use glass microspargers was demonstrated. Glass frit sparges were shown to be superior to polymer frit sparges at generating smaller, higher gas transfer, bubbles. The glass microsparger demonstrated the ability to support intensified perfusion cell culture theoretically through k_La, while not adversely affecting viable cell density for CHO cell culture. Even though the apparent k_La was higher than the sparger it replaced, the 16–40 μm microsparger was chosen based on better cell culture performance.

Pore size distributions of sintered microspargers are not necessarily indicative of actual bubble sizes. Factors such as

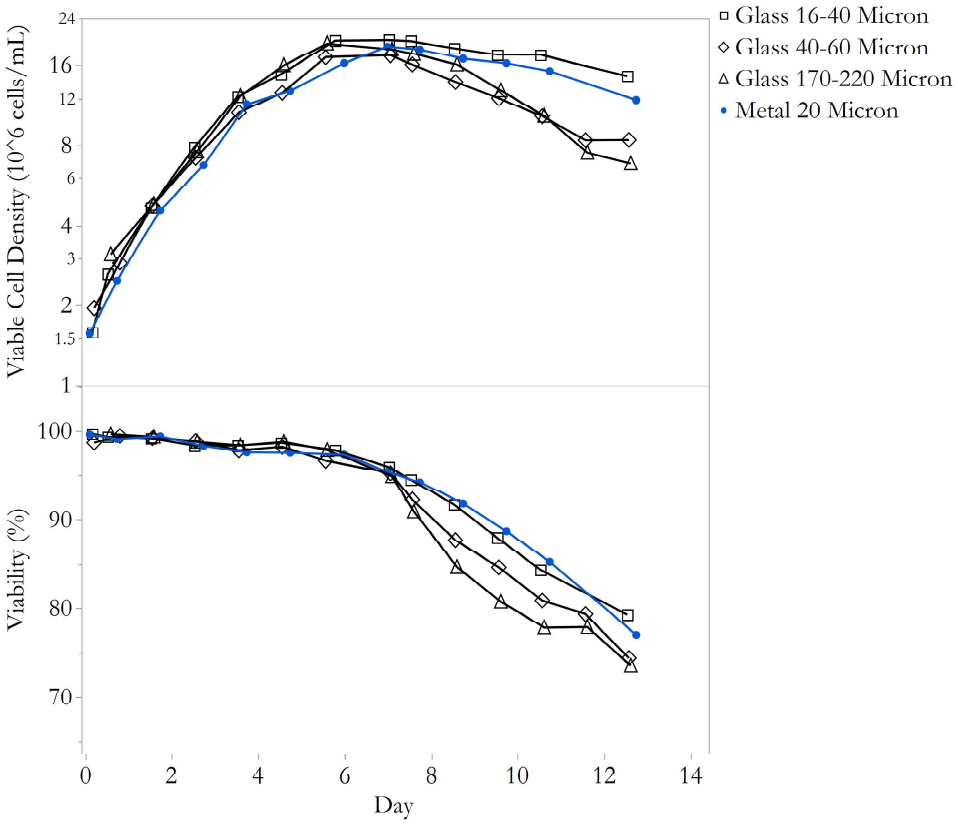

FIGURE 13 Viable cell density and viability for fed-batch cell culture runs with the microspargers as the main source of oxygen. The Glass 16–40 microsparger showed comparable cell culture performance to the 20 μm stainless steel. The cell culture runs using the 40–60 and 170–220 μm glass microspargers ended with ~35% lower viable cell density and ~7% lower viability.

wettability for materials of construction, medium composition, sparger surface roughness impact the bubble size distribution. In SUBs, particularly at the bench scale, the contact angle, or surface energy, has often not been considered for the design of sintered microspargers. The use of more hydrophilic materials, like glass, provides much better oxygen transfer rates. This could be applied to alternative designs, including spargers made with micron-sized laser-drilled holes.

NOTATION

C	BET constant
c_i	chord length
$d_{3,2}$	Sauter mean diameter
d_i	diameter length
k_La	oxygen mass transfer coefficient
$\frac{P}{P_0}$	relative pressure
$\frac{P}{\forall}$	power input per unit volume
V_α	volume of gas adsorbed
V_m	volume of gas adsorbed to produce an apparent monolayer
vvm	volume sparged per unit working volume per minute

AUTHOR CONTRIBUTIONS

William Tran: Writing – original draft (lead); writing – review and editing (equal). **T. Craig Seamans:** Writing – review and editing (equal). **John S. Bowers:** Writing – review and editing (equal).

ACKNOWLEDGMENTS

The authors thank Kevin Klejn at CerCell A/S for designing and fabricating the single use microspargers tested in this work. This work was funded by Merck Sharp & Dohme LLC, a subsidiary of Merck & Co., Inc., Rahway, NJ, USA, of which William Tran, Craig Seamans, and John Bowers are paid employees.

CONFLICT OF INTEREST STATEMENT

The authors declare no conflicts of interest.

PEER REVIEW

The peer review history for this article is available at https://www.webofscience.com/api/gateway/wos/peer-review/10.1002/btpr.3382.

DATA AVAILABILITY STATEMENT

The data that support the findings of this study are available from the corresponding author upon reasonable request.

ORCID

William Tran https://orcid.org/0009-0008-3420-3806

REFERENCES

1. Wesley DJ, Smith RM, Zimmerman WB, Howse JR. Influence of surface wettability on microbubble formation. *Langmuir*. 2016;32:1269-1278. doi:10.1021/acs.langmuir.5b03743
2. Lopes AG. Single-use in the biopharmaceutical industry: a review of current technology impact, challenges and limitations. *Food Bioprod Process*. 2015;93:98-114. doi:10.1016/j.fbp.2013.12.002

3. Mcandrew J, Kauffman G. Increasing Oxygen Transfer within the BIOne Single-Use Bioreactor Using a Microsparger; 2020, 212: 1-7. extension://elhekieabhbkpmcefcoobjddigjcaadp/https://www.distekinc.com/media/white-papers/bione-increasing-oxygen-transfer-using-a-microsparger-wp_212.pdf
4. Thermo Fisher Scientific. Introduction to mass transfer in single-use bioreactors. Thermo Fisher Scientific; 2020: 1-11. https://assets.thermofisher.com/TFS-Assets/BPD/Reference-Materials/introduction-mass-transfer-single-use-bioreactors-white-paper.pdf
5. Sieblist C, Aehle M, Pohlscheidt M, Jenzsch M, Lübbert A. A test facility for fritted spargers of production-scale-bioreactors. *Cytotechnology*. 2011;63(1):49-55. doi:10.1007/s10616-010-9325-6
6. Lin JN, Banerji SK, Yasuda H. Role of interfacial tensions in the formation and the detachment of air bubbles. *Langmuir*. 1994;10(3):936-942.
7. Wei M, Bowman RS, Wilson JL, Morrow NR. Wetting properties and stability of silane-treated glass exposed to water, air, and oil. *J Colloid Interface Sci*. 1993;157:154-159. doi:10.1006/jcis.1993.1170
8. Wesley DJ. The role of surface wettability on bubble formation in air-water systems. 2015; (University of Sheffield).
9. Alopaeus V, Koskinen J, Keskinen KI, Majander J. Simulation of the population balances for liquid-liquid systems in a nonideal stirred tank. Part 2-parameter fitting and the use of the multiblock model for dense dispersions. *Chem Eng Sci*. 2002;57:1815-1825. doi:10.1016/S0009-2509(02)00067-2
10. Maaß S, Wollny S, Voigt A, Kraume M. Experimental comparison of measurement techniques for drop size distributions in liquid/liquid dispersions. *Exp Fluids*. 2011;50:259-269. doi:10.1007/s00348-010-0918-9
11. Heath AR, Fawell PD, Bahri PA, Swift JD. Estimating average particle size by focused beam reflectance measurement (FBRM). *Part Part Syst Charact*. 2002;19:84. doi:10.1002/1521-4117(200205)19:2<84::AID-PPSC84>3.0.CO;2-1
12. Li M, Wilkinson D, Patchigolla K. Obtaining particle size distribution from chord length measurements. *Part Part Syst Charact*. 2006;23:170-174. doi:10.1002/ppsc.200601026
13. Wynn EJW. Relationship between particle-size and chord-length distributions in focused beam reflectance measurement: stability of direct inversion and weighting. *Powder Technol*. 2003;133:125-133. doi:10.1016/S0032-5910(03)00084-6
14. Camarasa E, Vial C, Poncin S, Wild G, Midoux N, Bouillard J. Influence of coalescence behaviour of the liquid and of gas sparging on hydrodynamics and bubble characteristics in a bubble column. *Chem Eng Process Process Intensif*. 1999;38(4-6):329-344.
15. Shah YT, Kelkar BG, Godbole SP, Deckwer W-D. Design parameters estimations for bubble column reactors. *AIChE J*. 1982;28:353-379. doi:10.1002/aic.690280302
16. Chisti Y. Animal-cell damage in sparged bioreactors. *Trends Biotechnol*. 2000;18:420-432. doi:10.1016/S0167-7799(00)01474-8
17. Mollet M, Godoy-Silva R, Berdugo C, Chalmers JJ. Acute hydrodynamic forces and apoptosis: a complex question. *Biotechnol Bioeng*. 2007;98:772-788. doi:10.1002/bit.21476
18. Ma N, Chalmers JJ, Auniņš JG, Zhou W, Xie L. Quantitative studies of cell-bubble interactions and cell damage at different pluronic F-68 and cell concentrations. *Biotechnol Prog*. 2004;20:1183-1191. doi:10.1021/bp0342405
19. Chaudhary G, Luo R, George M, Tescione L, Khetan A, Lin H. Understanding the effect of high gas entrance velocity on Chinese hamster ovary (CHO) cell culture performance and its implications on bioreactor scale-up and sparger design. *Biotechnol Bioeng*. 2020;117:1684-1695. doi:10.1002/bit.27314

How to cite this article: Tran W, Seamans TC, Bowers JS. Glass microspargers as effective frit spargers in single use bioreactors. *Biotechnol. Prog*. 2023;e3382. doi:10.1002/btpr.3382